Structural and magnetic properties of the osmium double perovskites $Ba_{2-x}Sr_xYOsO_6$

Paula Kayser, Sean Injac and Brendan J. Kennedy[*]

School of Chemistry, The University of Sydney, Sydney, NSW 2006, Australia

Thomas Vogt

Department of Chemistry and Biochemistry, 631 Sumter Street, University of South Carolina, Columbia, SC 29208, USA

Maxim Avdeev, Helen Maynard-Casely and Zhaoming Zhang

Australian Nuclear Science and Technology Organisation, Lucas Heights, NSW 2234, Australia

[*] E-Mail Brendan.Kennedy@Sydney.edu.au

Abstract

The crystal and magnetic structures of double perovskites of the type $Ba_{2-x}Sr_xYOsO_6$ have been studied by synchrotron X-ray and neutron powder diffraction methods, bulk magnetic susceptibility measurements and X-ray absorption spectroscopy. The structures were refined using a combined neutron and synchrotron data set and are based on ordered array of corner sharing YO_6 and OsO_6 octahedra, with the Ba/Sr cations being completely disordered. The structure evolves from cubic to monoclinic $Fm\bar{3}m \xrightarrow{x\sim0.6} I4/m \xrightarrow{x\sim1.0} I2/m \xrightarrow{x\sim1.6} P2_1/n$ as the Sr content is increased, due to the introduction of cooperative tilting of the octahedra. Bulk magnetic susceptibility measurements demonstrate the oxides are all antiferromagnets. The decrease in symmetry results in a, non-linear, increase in the Neel temperature. Low temperature neutron diffraction measurements of selected examples show these to be type-I-antiferromagnets. X-ray absorption spectra collected at the Os L_3- and L_2-edges confirm the Os is pentavalent in all cases, and there is no detectable change in the covalency of the Os cation as the A-cation changes. Analysis of the L_3:L_2 branching ratio shows that the spin-orbit coupling is constant and insignificant across the series.

INTRODUCTION

Transition metal containing double perovskite oxides, with the general formula $A_2BB'O_6$, are the subject of considerable current interest. In particular double perovskite containing metals with unfilled $5d$ shells have been found to display fascinating and attractive physical properties, including colossal magnetoresistance (e.g., Sr_2FeWO_6 [1]), optical properties (e.g., Sr_2CrReO_6 [2]), high T_N ferrimagnetism (e.g., Sr_2CrOsO_6 [3]), half metallicity (e.g., A_2CrWO_6 [4]), and metallicity (e.g., Sr_2CrReO_6 [5]). The $A_2BB'O_6$ double perovskite structure consists of a corner connected network of BO_6 and $B'O_6$ octahedra, which alternate in all three directions, so that each BO_6 octahedron is connected only to $B'O_6$ octahedra and vice versa[6, 7]. Consequently the structure is a combination of two interpenetrating face centred cubic lattices, each of which exhibits intrinsic geometric frustration [8, 9]. Compared to simpler ABO_3 ternary perovskites, the ordering of the B and B' cations strongly influences both the electronic structure and the magnetic coupling, resulting in an increased variety of magnetic exchange interactions in the double perovskite structure.

The subtle competition between different exchange interactions in double perovskites can lead to exotic magnetic phases, exemplified by antiferromagnetic (AFM) transitions in the $3d–5d$ double-perovskites Sr_2CoOsO_6 [10, 11] and Sr_2FeOsO_6 [12, 13]. In these oxides the long-range Os-B'-Os coupling is mediated by the magnetic B' cation $Co(3d^7)$/$Fe(3d^5)$ and is surprisingly large. Even when the second metal does not contain unpaired d-electrons it can play a significant role in moderating the magnetic exchange interactions between the two Os cations. This is illustrated in the two oxides Sr_2YOsO_6 and Sr_2InOsO_6 that have AFM transition temperatures of $T_N = 53$ and 27 K, respectively [14, 15]. Y^{3+} has a $4d^0$ open-shell configuration whereas In^{3+} has a closed-shell $4d^{10}$ configuration. Density functional theory (DFT) calculations reveal that the short-range Os-Os interactions are much stronger in Sr_2YOsO_6 than the long-range ones, unlike in Sr_2CoOsO_6 [10, 11] and Sr_2FeOsO_6 [12, 13]. Hybridization between the Os- $5d$ and B'- $4d$ orbitals is much smaller in the d^{10} closed-shell case than that in the d^0 open-shell case, reducing the amplitudes of Os-Os coupling in Sr_2InOsO_6 compared to those in Sr_2YOsO_6.

Magnetic exchange interactions, and the consequent magnetic ground states, in double perovskites are known to be sensitive to the effect of chemical pressure that can be tuned by altering the size of the larger A-site cation. Both Sr_2CrOsO_6 and Ca_2CrOsO_6 are ferrimagnets, however replacing the Ca with the larger Sr cation significantly increases T_C from 490 K to

660 K [16-18]. Ca_2ScOsO_6 has a Neel Temperature of 69 K [19]. Substituting Ba for Sr in ALaNiOsO$_6$ (A = Sr, Ba), results in a change in the Weiss Temperature (Θ_W) from negative to positive as a consequence of the decrease of structural distortions.[20] SOC in $4d$ and $5d$ oxides has emerged as another key factor contributing to the unusual magnetic properties of oxides containing metals such as Os. In $5d$ oxides the relativistic SOC is of a similar magnitude to crystal field effects and electronic correlations (Hubbard U) [21]. A consequence of these often finely balanced interactions in $5d$ oxides is the emergence unexpected phenomena, such as the spin orbit coupling dominated $j_{eff} = 1/2$ Mott-like insulating state observed in Sr_2IrO_4 [22] and magnetic metal insulator transitions in pyrochlore iridates and osmates [23].

In the present work we report the synthesis and characterization of the series of Os containing double perovskites $Ba_{2-x}Sr_xYOsO_6$. Since the $4d$ and $5d$ orbitals are more spatially extended than the 3d orbital, in oxides containing $4d$ and especially $5d$ elements, the Coulomb interactions are typically weaker resulting in a large splitting of the crystal field and increased sensitivity to lattice distortions. In addition to the crystal field splitting, the t_{2g} orbitals may be modified into $J_{eff} = 1/2, 3/2$ bands through the effects of strong SOC. The combination of these factors, make this system a perfect candidate to study competition between lattice distortions and SOC. We demonstrate through the use of X-ray and neutron diffraction coupled with magnetic susceptibility measurements that chemical pressure, introduced by the use of a smaller A-site cation, alters the structure and details of the magnetic properties of these Os double perovskites. The structural studies allow us to establish the importance of geometric factors in a series with a constant magnetic cation. X-ray absorption spectroscopy at the Os L-edge has been used to establish the oxidation state of the Os cation and to probe the relationship between changes in the structure on the SOC and magnetic properties across this series.

EXPERIMENTAL

Polycrystalline samples of 11 members of the solid solution $Ba_{2-x}Sr_xYOsO_6$ ($0 \leq x \leq 2$) were prepared by conventional solid-state methods. Stoichiometric amounts of BaO_2 (Sigma Aldrich 95%), SrO_2 (Sigma Aldrich 958%), Y_2O_3 (Aithaca, 99.999%) and Os powder (Aithaca, 99.9%) (10% excess) were finely mixed as an acetone slurry in an agate mortar and heated in air at 1150 ºC for 24 h with intermediate re-grindings. Due to the possibility of producing toxic OsO_4 gas, the entire synthesis was carried out in a fumehood using sealed alumina crucibles. Reaction progress was followed by X-ray diffraction (XRD), using a

PANalytical X'Pert PRO X-ray diffractometer in Bragg-Brentano reflection geometry with Cu Kα radiation (λ=1.5418 Å) equipped with a PIXcel solid-state detector.

Synchrotron X-ray powder diffraction (S-XRD) data were collected over the angular range 5 < 2θ < 85°, using X-rays of wavelength 0.824530 Å, calibrated using a NIST SRM 660b LaB_6 standard, on the powder diffractometer at Beamline BL-10 of the Australian Synchrotron [24]. The samples were housed in 0.2-mm-diameter capillaries, which were rotated during the measurements. The data were obtained using a bank of 16 Mythen detectors, each of which covers 5 degrees of data. Diffraction data were collected for 5 min at each of the two detector positions, to avoid gaps in the data from the individual modules. Neutron powder diffraction experiments were carried out at ANSTO's OPAL facility at Lucas Heights. Room temperature neutron powder diffraction (NPD) data were acquired using the high-intensity diffractometer Wombat[25] and low-temperature NPD experiments were performed in the high-resolution powder diffractometer Echidna[26] in order to determine the magnetic structure of selected samples. The wavelength of the neutrons, obtained using a vertically focussing Ge 115 and Ge 331 monocromator, was 1.498 Å and 2.439 Å respectively. Approximately 1.5 g samples were placed in thin-walled vanadium holders. The S-XRD and NPD data were refined by the Rietveld method [27] using the FULLPROF refinement program [28]. A pseudo-Voigt function was chosen to generate the line shape of the diffraction peaks. No regions were excluded in the refinement. The following parameters were refined in the final analysis: scale factor, zero-point error, background (12 term shifted Chebyschev) coefficients, lattice parameters, positional coordinates and isotropic atomic displacement.

A Quantum Design PPMS system was used to collect direct-current magnetic susceptibility data, measured both in zero-field-cooled (ZFC) and field-cooled (FC) modes in the $2 \leq T \leq 300$ K range under an applied magnetic field of 0.1 T.

X-ray absorption near edge structure (XANES) spectra were measured at the Os L_2 and L_3-edges on beamline BL-12 at the Australian Synchrotron[29]. The measurements were performed at room temperature in transmission mode using argon-filled ionization chambers. The beam intensity (I^0) was monitored by a flow through ionization chamber located upstream from the sample. XANES spectra were collected by a second ionization chamber placed immediately after the sample. A third ionization chamber was placed downstream to simultaneously measure a standard spectrum of Ba_2YOsO_6. Appropriate amounts of the

sample and BN were mixed, manually pressed between two Kapton tapes and positioned directly in front of the X-ray beam. Energy steps as small as 0.25 eV were employed near the absorption edge with a counting time of 1 s per step. The energy scale of the monochromator was calibrated using the L_3-edge of a Pt foil at 11562.7 eV, and the Ba_2YOsO_6 reference spectra were used to align scans from different samples during the experiment. All XANES data were analyzed using the Athena software program [30].

RESULTS AND DISCUSION

Crystal Structures. The 11 $Ba_{2-x}Sr_xYOsO_6$ ($0 < x < 2$) samples were obtained as black well-crystallized powders. In a first visual analysis of the S-XRD data, it was observed that all of the patterns are characteristic of a perovskite-type structure, showing sharp and well defined superstructure reflections due to the rock-salt arrangement of the Y^{3+} and Os^{5+} cations. As detailed by Anderson *et al.*[6] establishing long-range 1:1 *B*-site ordering in double perovskites requires a difference in the charge and size difference between the two cations. The combination Y^{3+} (0.900 Å) and Os^{5+} (0.575 Å) is sufficient to stabilize a high degree of cation ordering. In addition, the high covalency of the Os-O bonds, compared with the corresponding Y-O bond, reinforces the cation ordering in this system since the anion polarization is maximum for Y-O-Os rather than for Y(Os)-O-Y(Os). At higher Sr compositions, additional superlattice reflections corresponding to the distortion of the oxygen sublattice were identified. These reflections indicate the presence of cooperative tilting of the corner sharing BO_6 octahedra, and will be discussed in detail in the next paragraphs.

In order to assign the correct symmetry, a combined structural refinement of high resolution S-XRD and NPD was carried out at room temperature. Whilst the narrower peak widths in the S-XRD patterns provide high precision in determining the cell metric and revealed splitting of selected reflections indicative of symmetry lowering, the refined positional parameters of the light oxygen anions were of relatively low precision reflecting the presence of heavy Os (Z = 76) and Ba cations (Z =56). Consequently NPD was an essential technique to refine accurate and precise anion positions. As a first step, the nuclear structure was refined from the synchrotron data and subsequently the veracity of the obtained lattice parameters was confirmed by Rietveld refinement against the combined of S-XRD and NPD data sets. The difference in the number of electrons as well as in the neutron scattering length between the Y (7.75 fm) and Os (10.7 fm) atoms provided considerable sensitivity to Y-Os ordering over the two *B*-sites. The refined anti-site occupancy of Y at Os positions and

vice versa indicates that all the samples are fully ordered. It is worth recalling that for double perovskites the cation ordering results in the same additional *R*-point reflections as does out-of-phase tilting of the octahedra, consequently it is necessary to consider the intensity of these to establish their origin. The in-phase tilting is associated with an *M*-point mode while coupling of the out-of-phase tilts and the displacement of the *A*-type cation gives rise to *X*-point reflections [31, 32]. The refinement of the oxygen occupancy shows that there are no oxygen vacancies in any of the samples. Small amounts of Y_2O_3 (<2%) and SrY_2O_4 (<5%) oxides were identified in some samples and these were included as secondary phases in the refinements. These phases are likely formed due to the evaporation of small amounts of Os during the synthesis. Four polytypes were identified in the series and a representative Rietveld refinement for each symmetry (x = 0.0, 0.6, 1.0, 1.8) is shown in Figure 1. The refined parameters, including unit-cell parameters, volume, atomic displacement parameters, atomic positions and selected bond distances and angles are summarized in Table 1 and 2.
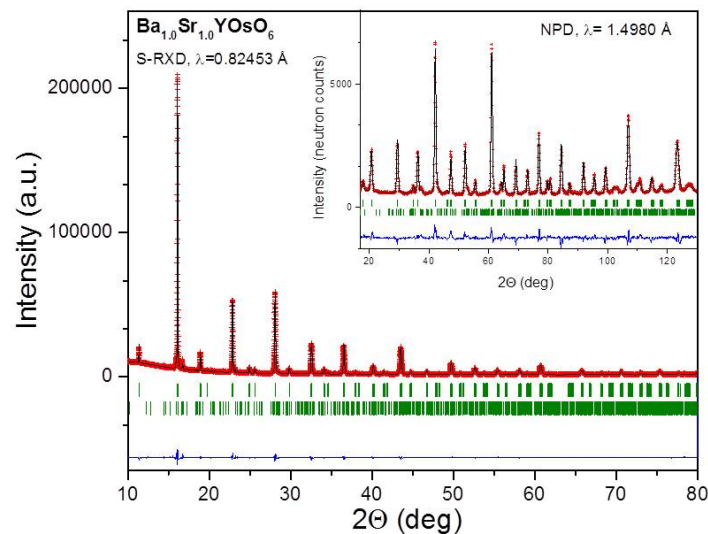

Figure 1. Combined S-XRD-NPD Rietveld refinement profiles for $Ba_{1.0}Sr_{1.0}YOsO_6$ at room temperature. The symbols are the experimental data, the solid line is the fit to the profile, the first series of Bragg reflections correspond to the main perovskite phase (S.G: *I2/m*) and the second one corresponds to Y_2O_3. The S-XRD data were collected at λ = 0.82453 Å and the NPD data (shown as insets) collected on the high intensity Wombat diffractometer at λ = 1.4980 Å

For the end member Ba_2YOsO_6 oxide the S-XRD and NPD data were fitted in the cubic space group $Fm\bar{3}m$ (No. 225), with the unit-cell related to a_p (parameter of primitive cubic perovskite) as $a = 2a_p$. As shown in Figure 2a, the doubling of the unit-cell is confirmed by the presence of R-point reflections (odd-odd-odd reflections). The refined cell-parameter a= 8.35409(1) Å is in good agreement with that previously reported by Kermarrec *et al.* (a= 8.3541(4) Å) [8]. The introduction of Sr at the A-site causes the tolerance factor, $t = \frac{(r_A + r_O)}{\sqrt{2}(r_B + r_O)}$, where r_A, r_B, and r_O correspond to the radius of the A and average of the two B site cations and the oxygen anions respectively, to decrease resulting in cooperative tilting of the BO_6 octahedra. As shown in Figure 2b, which displays portions of the room temperature NPD profiles, there is a noticeable increase in the intensity of the R-point reflections at $x = 0.6$ as a result of the introduction of out-of-phase tilting of the corner sharing octahedra. Examination of the S-XRD profile at $x = 0.6$ suggests that the structure is tetragonal. According to Howard's group theory analysis [31], the tetragonal structure that only contains out-of-phase tilts is in space group $I4/m$ (No. 87) and this was used in the analysis of the diffraction data for $Ba_{1.4}Sr_{0.6}YOsO_6$. The transition from $Fm\bar{3}m$ to $I4/m$ involves the introduction of out-of-phase octahedral tilting along the [001] direction and the transformation is allowed to be continuous (second-order transition). Further doping with Sr at the A-site results in a second phase transition, which has been identified based on the c/a ratio. At $x = 0.6$ the pseudo-tetragonal ratio is $\frac{c_p}{a_p} > 1$ while at $x = 1.0$ it reverses $\frac{c_p}{a_p} < 1$ indicating a reorientation of the octahedral tilting[31]. Again only R-point reflections are evident in the NPD and S-XRD profiles. In the composition range $x = 1.0$-1.4 the crystal structure of all the compounds has been successfully refined in the monoclinic space group *I2/m* (No. 12). The transition from *I4/m* to *I2/m* involves a change in the direction of the octahedral tilt from about the *c*-axis in the former symmetry to along the [110] direction in the monoclinic structure. Group theory shows that this transition must be first order[31]. At still higher Sr contents ($x \geq 1.6$), additional superlattice peaks at 2Θ ~ 34° and 40° are observed (Figure 2b). These are identified as *M*-point reflections which demonstrate the existence of in-phase octahedral tilting. The structure of these samples ($x = 1.6$-2.0) is described in space group *P2₁/n*, which shows out-of-phase tilting along the [100] and [010] directions and in-phase-tilt along the [001] direction with respect to the pseudo-cubic perovskite cell. The nature of this transformation, which only introduces an extra tilt along the *c*-axis, is allowed to be second-order. The unit-cell parameters of the Sr_2YOsO_6 ($a = 5.78499(8)$, $b = 5.80075(7)$ and $c = 8.1925(1)$ Å) obtained in this work are very similar to those reported by Paul *et al.* (*a*

$= 5.7817(1)$ Å, $b = 5.8018(1)$ Å and $c = 8.1877(1)$ Å) [14]. The observed phase transition sequence: $Fm\overline{3}m \rightarrow I4/m \rightarrow I2/m \rightarrow P2_1/n$ has been previously reported in the analogous solid solutions A_2YBO_6 for $B = $ Ru and Ir [33, 34], and in a number of related systems including A_2CoWO_6 [35], A_2NiWO_6 [36] and A_2InTaO_6 [37].
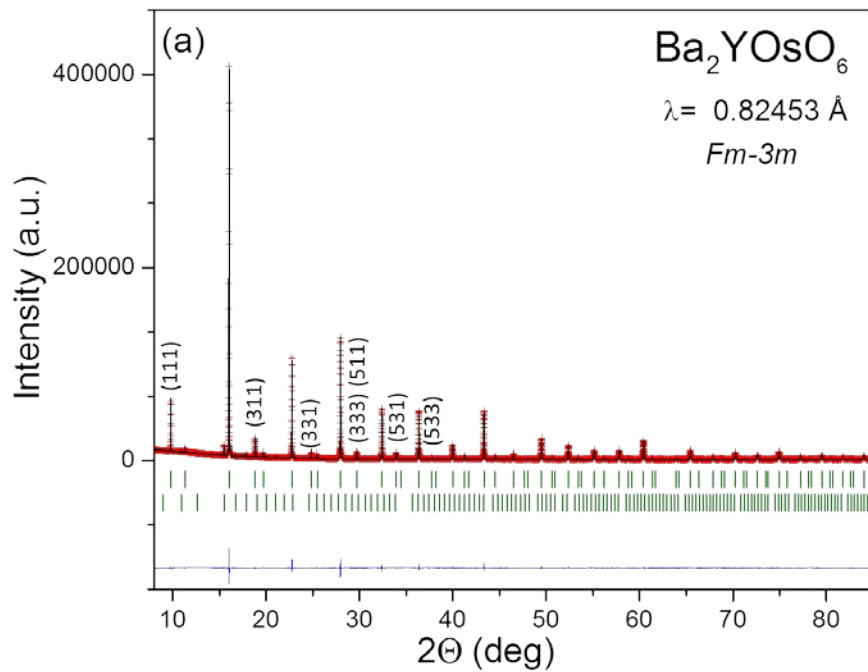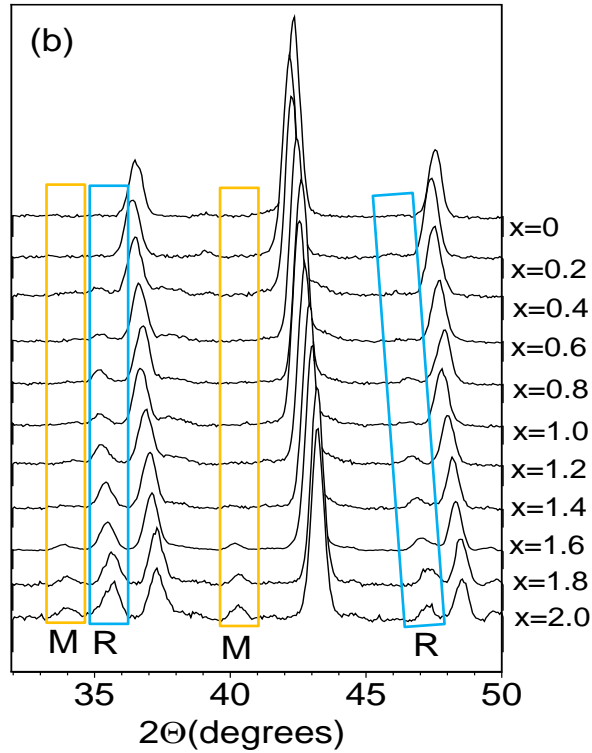
Figure 2. (a) S-XRD Rietveld refinement profile for Ba_2YOsO_6. The *R*-point reflections (odd-odd-odd) indicate the doubling of the unit-cell. (b) Portions of the NPD patterns for $Ba_{2-x}Sr_xYOsO_6$ from x = 0 (top) to x = 2 (bottom) highlighting the development of superlattice reflections associated with cooperative tilting of the corner-sharing octahedra.

Magnetic Properties. The thermal evolution of the magnetic susceptibilities for selected members of the solid solution $Ba_{2-x}Sr_xYOsO6$ (x = 0.2, 0.8, 1.0, 1.2, 1.8) is displayed in Figure 3. In all of the cases the curves show a well-defined maximum corresponding to an AFM transition. Depending on the composition, and therefore on the crystal structure of each compound, the Neel temperature generally increases from 54 to 74 K as the Ba content, and hence symmetry, is increased, although this is clearly not a simple relationship. The corresponding values reported previously for Ba_2YOsO_6 (x = 0) and Sr_2YOsO_6 (x = 2) are 70 and 53 K respectively [8, 14]. The data for x = 1.2 shows a second weak anomaly that is believe to be due to trace amounts of a magnetic impurity that were not apparent in the diffraction data. There is no divergence between the ZFC and the FC curves for any of the samples, except at very low temperatures that may indicate a slight canting of the spins. At 4.5 K the isothermal magnetization curves (Figure 4) show an almost linear response with no hysteresis

10

or remnant magnetization. The shapes of all of the curves are characteristic of the behavior of AFM materials. We note that estimating the Neel temperature in double perovskites such as these is better achieved combining bulk susceptibility with either neutron diffraction or heat capacity measurements. Due to instrument availability and the challenges in preparing well sintered samples such measurements were not feasible for this series.
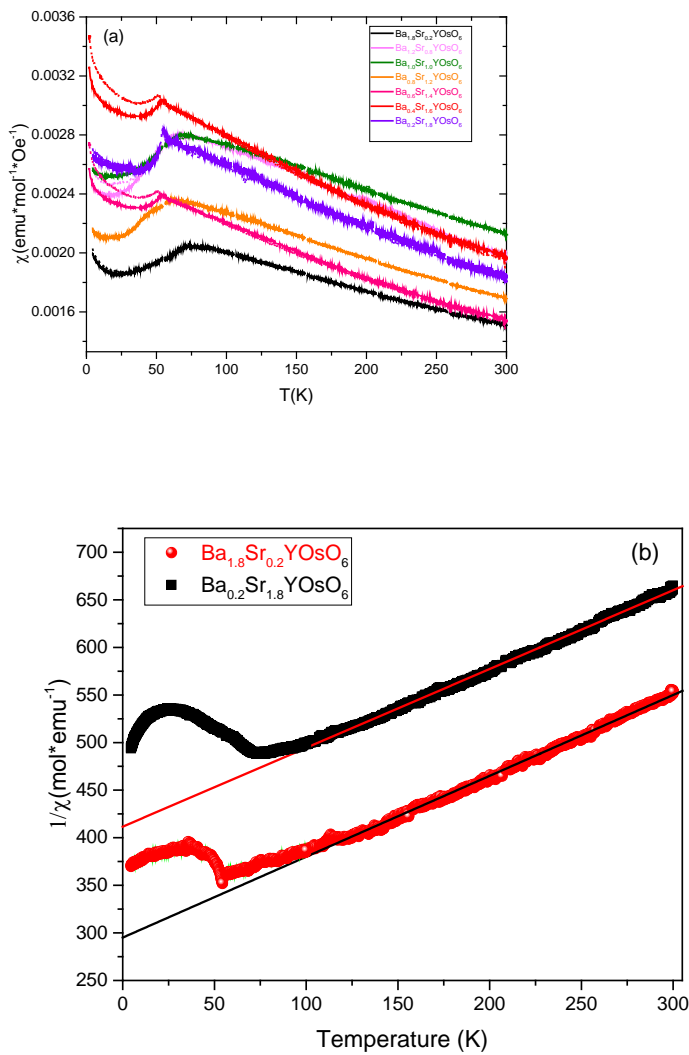

Figure 3. Thermal evolution of (a) dc magnetic susceptibility and (b) inverse susceptibility for selected members in the series $Ba_{2-x}Sr_xYOsO_6$ measured at 0.1 T.
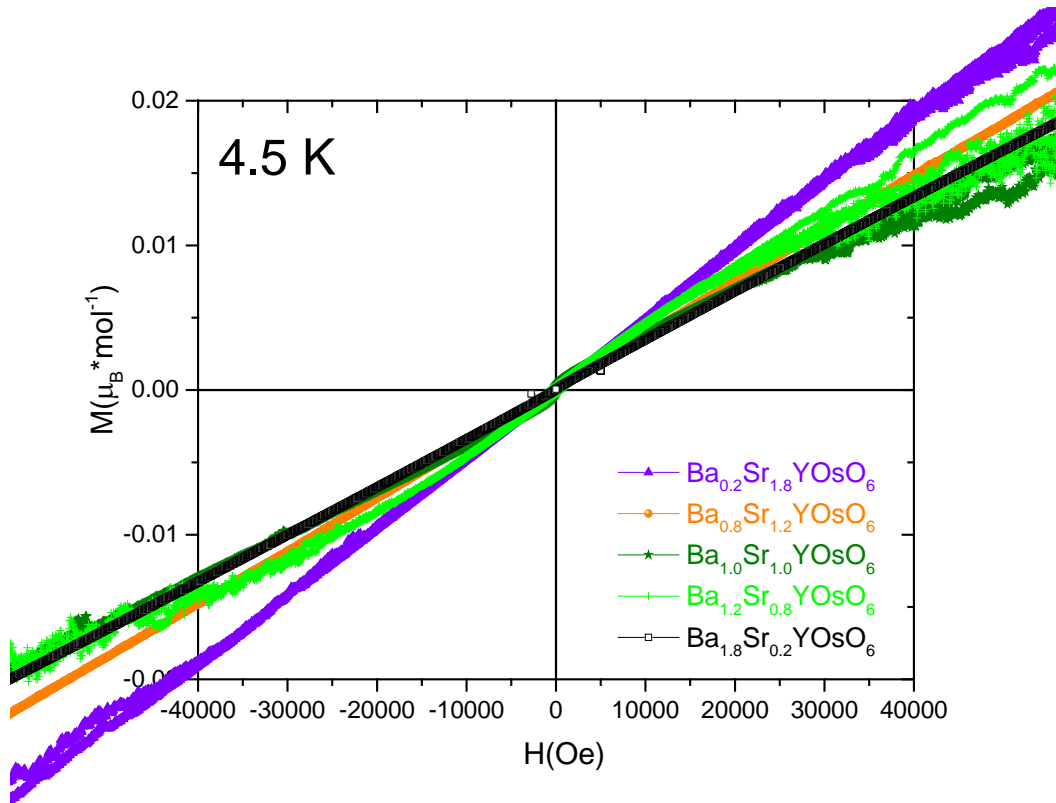
Figure 4. Magnetization versus magnetic field isotherms selected members in the series $Ba_{2-x}Sr_xYOsO_6$ measured at 4.5 K measured under a magnetic field ranging from −4000 to 4000 Oe.

Above the magnetic ordering temperature, the reciprocal susceptibility curve (Figure 3b) follows the Curie-Weiss law $\chi = C/(T - \theta)$. The effective magnetic moment, obtained as $2.84\sqrt{C}$ (where C represents the Curie constant) from a linear fit in the temperature range 200-300 K, varies between 3.0(1) - 2.96(3) μ_B. Kermarrec et al.[8] reported a significantly higher value of the effective magnetic moment for Ba_2YOsO_6 (μ = 3.93 μ_B). These workers however noted that their Curie-Weiss fitting yielded an extremely large negative θ_{cw} (-717 K), indicating that the paramagnetic region in their sample was above 300 K. In contrast Paul et al. reported μ = 3.45 μ_B for Sr_2YOsO_6 with a much reduced negative value of θ_{cw} (-337 K). These values are below the spin only magnetic moment for a Os^{5+} (t_{2g}^3, S=3/2) ion of 3.87 μ_B.

The difference between the observed and calculated magnetic moments is attributed to SOC effects, which for a half-filled t_{2g}^3 electron configuration should lead to a reduction of the moments from the spin-only values [15]. A further effect is the large covalence existing in

these systems which is expected to lead to a reduction in the magnetic moment. The large negative Weiss temperatures in the compounds, which varies between -350 and -530 K confirms that the magnetic interactions are predominantly antiferromagnetic-and suggests the presence of moderate frustration with a ratio $|\theta_{cw}|/T_N \sim$ 4-8 [38]. That θ_{cw} did not vary systematically with composition is believed to be a consequence of the frustration in the system. The face-centred-cubic (fcc) lattice, can be viewed as composed of edge-sharing Os tetrahedra, which is geometrically frustrated in the presence of AFM interactions [8, 21]. Whilst the frustration index cannot be used as the unique criteria to predict magnetic frustration, it provides a strong indication of the nature of exchange interactions in the system.

Magnetic Structure. The magnetic structure of the two selected members (x = 1.0 and 1.2) of the solid solution $Ba_{2-x}Sr_xYOsO_6$ have been investigated using neutron powder diffraction patterns measured at below the magnetic ordering temperature. Additional variable temperature data were measured for $Ba_{1.0}Sr_{1.0}YOsO_6$ from 3 to 75 K (inset of Figure 5). Careful examination of the NPD data measured at 3K provided no evidence for any *M*-point reflections, which are diagnostic of the presence of in-phase tilting of the octahedra, and it was concluded that the structure remains monoclinic in $I2/m$ down to 3 K. As evident in Figure 5 as the temperature is reduced from 70 K a number of additional reflections emerge at low angles ($2\Theta\sim16°$ and $24°$) as a consequence of the onset of long-range magnetic order. This magnetic ordering temperature range is in good agreement with the corresponding Neel temperature obtained from bulk susceptibility measurements described above (T_N = 69 K). For both samples, analysis of the positions of the magnetic reflections, using K_SEARCH in FullProf,[28] indicated that the corresponding magnetic structure was defined by the propagation vector $\mathbf{k}$ = (½ ½ 0), which means that the additional magnetic peaks could be indexed by a supercell where the *a*- and *b*-axes are doubled with respect to the nuclear cell. To determine the possible magnetic structure models compatible with the monoclinic *I2/m* space group, representation analysis was employed following the procedure described by Bertaut [39]. The irreproducible representations and the corresponding basis vectors associated with the Os^{5+} sublattice were generated using BasIrep as implemented in Fullprof. For the space group *I2/m* and the propagation vector $\mathbf{k}$ = (½ ½ 0), the only irreducible representation of the small group G_k is Γ^2 and the basis vectors for the magnetic atoms located at (000) and (½ ½ ½) are (100), (010) and (001). The Rietveld refinement of the nuclear and magnetic structure, shown in Figure 5, yielded in a magnetic moment of 1.5(2) and 1.64(5) μ_B for $Ba_{1.0}Sr_{1.0}YOsO_6$ and $Ba_{0.8}Sr_{1.2}YOsO_6$ respectively, with the spins defined along the *c*-axis.

Figure 6 displays a schematic view of the structure which can be described as an AFM coupling of ferromagnetic (110) planes indicative of a AFM1 structure. The magnetic ground state described by $\mathbf{k} = (\frac{1}{2}\ \frac{1}{2}\ 0)$ is relatively rare compared with the k = (000) ground state, although it was described recently for La_2LiOsO_6 [21]. Given the two have similar near neighbor and next nearest neighbor interaction they are expected to be very similar in energy and it is unclear what, if any, significance lies in this.
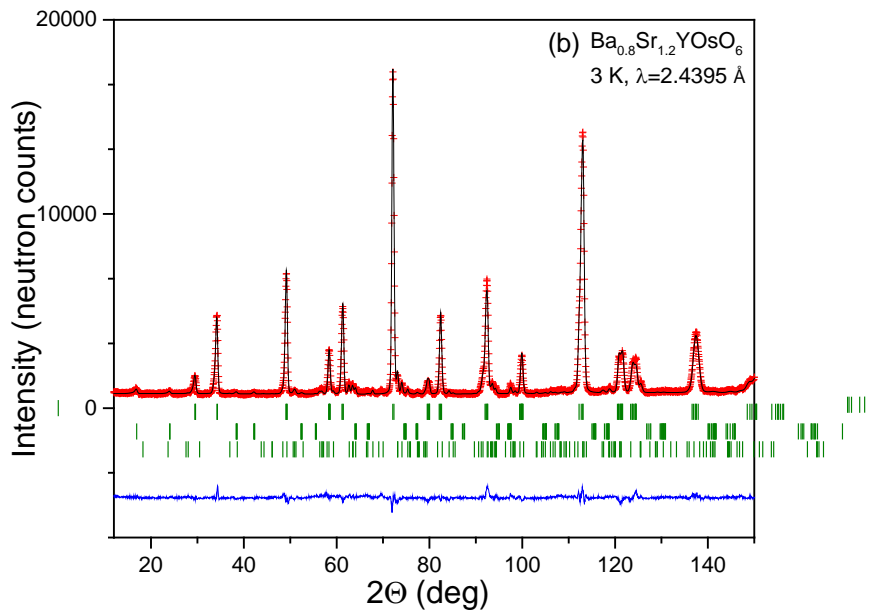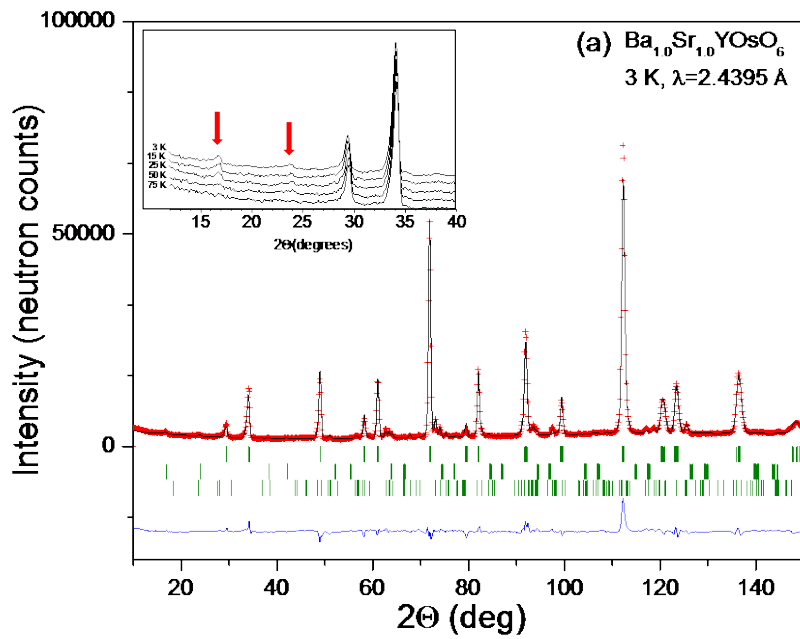
Figure 5. Observed (crosses), calculated (solid line), and difference (bottom) NPD Rietveld profiles for (a) $Ba_{1.0}Sr_{1.0}YOsO_6$ and (b) $Ba_{0.8}Sr_{1.2}YOsO_6$ at 3 K collected at the high resolution Echidna diffractometer. The first and the second series of Bragg reflections correspond to the nuclear and magnetic structure of main perovskite phase and the third one

corresponds to Y_2O_3. The inset of (a) shows the thermal evolution of NPD patterns and the red arrows indicate the position of the magnetic reflections.
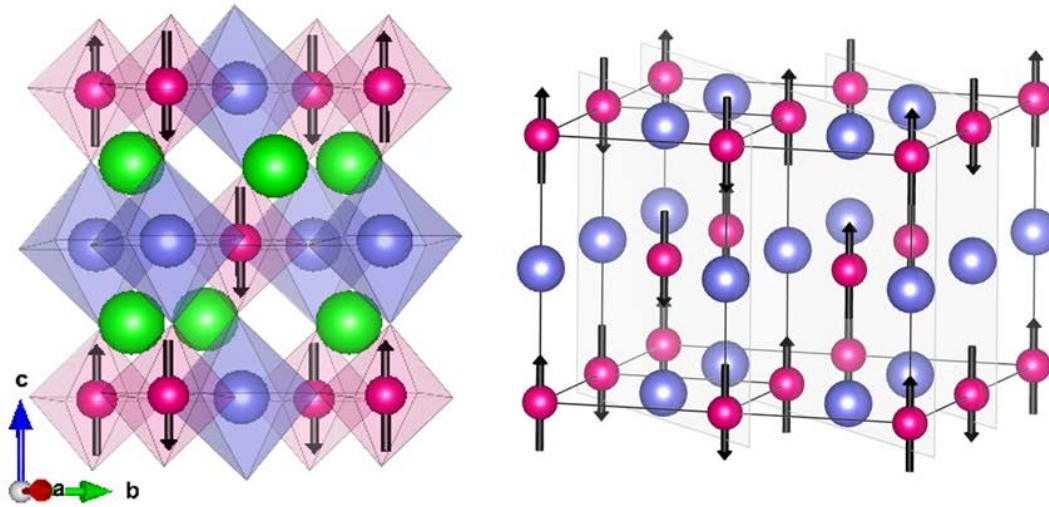

Figure 6. Schematic view of the magnetic structure in the $I2/m$ structured $Ba_{2-x}Sr_xYOsO_6$ (x = 0.8 and 1.0) oxides. The large green spheres represent the A-cations and the blue and pink spheres correspond to the Y and Os cations respectively. The arrows indicate the direction of the Os magnetic moments.

X-ray absorption near-edge structure (XANES) results.

XANES spectra were collected at the Os L_3- and L_2-edges from all eleven samples in the $Ba_{2-x}Sr_xYOsO_6$ series. Figure 7 shows the normalized Os L_3- and L_2-edge XANES spectra of $BaSrYOsO_6$ corresponding to dipole transitions of $2p_{3/2} \rightarrow 5d_{3/2,5/2}$ and $2p_{1/2} \rightarrow 5d_{3/2,5/2}$ respectively (the continuum step at the L_3 and L_2 absorption edge is normalized to one and to a half respectively, reflecting the difference in the number of initial core-electron states available for the L_3 and L_2 absorption processes). There is essentially no change in the XANES spectra as the content of Sr changes from 0 to 2, as evident in Figure 8, confirming that the Os oxidation state remains 5+ throughout the solid solution $Ba_{2-x}Sr_xYOsO_6$. For Os atoms coordinated to six oxygen atoms (*i.e.*, in an octahedral or slightly distorted octahedral environment), the Os L_3-edge XANES spectra consist of two components corresponding to the t_{2g} and e_g orbitals due to crystal field splitting (CFS) of the Os($5d$) states, similar to the XANES spectra at the L_3-edge from octahedrally coordinated Zr or Hf in pyrochlore materials [40][41]. Although the two peaks corresponding to t_{2g} and e_g orbitals are well resolved

at the Zr L_3-edge, they are not resolved at the Hf or Os L_3-edge due to larger natural widths associated with higher-energy atomic levels of Hf(5d) or Os(5d) than Zr(4d) [42]. The CFS of the Os($5d$) states can, however, still be estimated as ~3.9 eV from the difference between the two 'valleys' in the second derivative spectra (inset of Figure 8) [41, 43]. It should be mentioned that very slight displacements of the e_g peak were observed at the Y L_3-edge in the analogous system of $Ba_{2-x}Sr_xYRuO_6$ as a function of Sr content,[33] which were not observed at the Os L_3-edge in the current series of $Ba_{2-x}Sr_xYOsO_6$. Overlapping of the t_{2g} and e_g peaks of the Os(5d) states prevent such subtle changes being be detected.
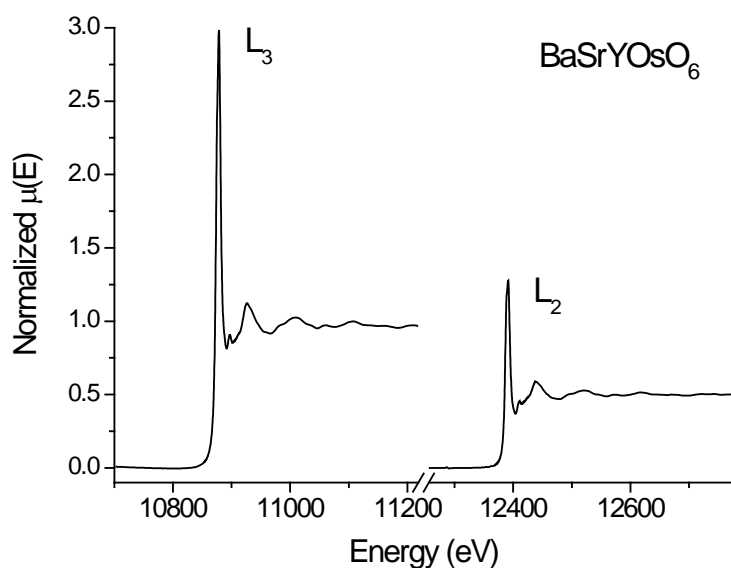

Figure 7. Normalized XANES spectra obtained from $BaSrYOsO_6$ at the Os L_3 and L_2 absorption edges.
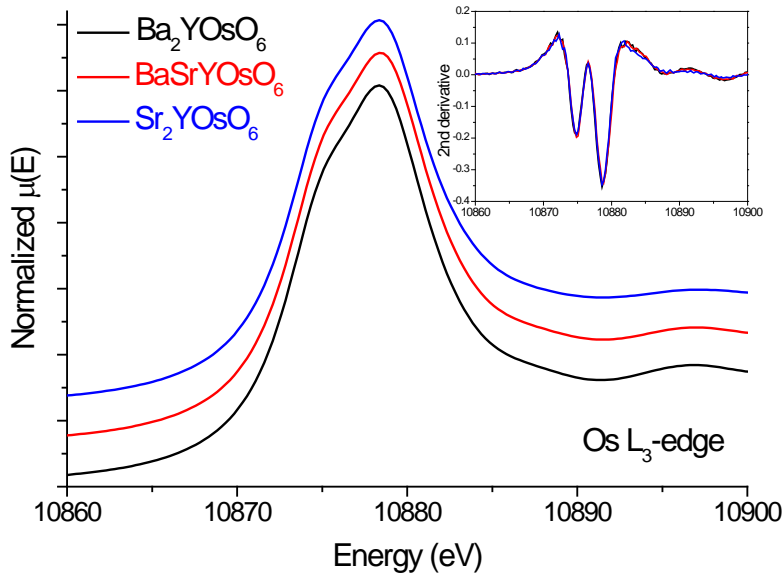
Figure 8. Normalized XANES spectra collected at the Os L_3-edge from Ba_2YOsO_6 (black), $BaSrYOsO_6$ (red) and Sr_2YOsO_6 (blue) with their second derivatives plotted in the inset.

Furthermore, X-ray absorption spectroscopy provides useful information to probe the SOC interactions of a material, and the strength of the coupling can be quantitatively extracted from XANES spectra by determining the intensity ratio of the white lines at the L_3 and L_2 edges (*i.e.*, branching ratio BR= I(L_3)/I(L_2)). Branching ratios significantly greater than the statistical value of 2 indicate the presence of a strong coupling between the local orbital and spin moments. This method, proposed by Thole and van der Laan, [44] has been successfully used to study the influence of SOC interactions in the ground state of several iridium-based compounds [43, 45]. Since SOC interactions are potentially present in Os-containing compounds, and it was observed that the magnetic moments (as obtained from the analysis of the NPD data) are lower than the expected values in the current $Ba_{2-x}Sr_xYOsO_6$ system, the branching ratios have been calculated for all the samples in this series. It is shown that the BR remains constant throughout the series (BR ~ 2.2 using the 'moderate' method as shown in Figure 2 of Cho *et al.* [46]) and this value of the BRs corresponds to the statistical value within experimental error), which means that the SOC effect is minimal in this system. Nevertheless the inelastic neutron data analysis reported by Kermarrec *et al.* [8] reveals a spin gap to the spin-wave excitations of 19(2) meV for Ba_2YOsO_6, which is unexpected for an orbitally quenched t_{2g}^3 electronic configuration, and these authors concluded SOC is

important in this compound. Evidently additional studies are required to reconcile these differences.

DISCUSSION

High resolution S-XRD and NPD data have been measured, at room temperature for 11 members in the series $Ba_{2-x}S_xYOsO_6$. Examination of the superlattice reflections and of the diagnostic peak splitting enabled the symmetry and space groups of these oxides to be established. Subsequently the structures were refined using combined S-XRD/NPD data sets. All oxides exhibited a rock-salt like ordering of the Y^{3+} and Os^{5+} cations. As illustrated in Figure 9, an increase in the Sr-content at the A-site of the double perovskite generally resulted in a reduction in the unit-cell parameters and volume, although the results for the two Ba rich oxides, Ba_2YOsO_6 and $Ba_{1.8}Sr_{0.2}YOsO_6$ are clearly anomalous. We note that the diffraction peaks in the SXRD profiles for the $x = 0.2$ and 0.4 samples were somewhat broader than for other members of the series. The unit cell volumes obtained for the two end-member oxides Ba_2YOsO_6 and Sr_2YOsO_6 in the current work are in excellent agreement with published values, and in particular the refined cell parameter for Ba_2YOsO_6 of 8.35409(1) Å is in excellent agreement with that reported by Kermarrec *et al.*, 8.3541(4) Å. The values for Ba_2YOsO_6 and $Ba_{1.8}Sr_{0.2}YOsO_6$ are reproducible demonstrating this is not an experimental artifact. Deviations from Vegards law are not uncommon and can arise from either local ordering of the dopant cation or magnetic effects. In the present work we are unable to establish if either of these effects is responsible, but the peak broadening suggests the presence of additional strains that may be a consequence of local disorder [47] although strain fields around dopant atoms typically only extend across 2 – 3 unit cells with effective relaxation distances of ~ 16 – 18 Å in diameter[48].

The average Os-O and Y-O bond distances (Table 2) were remarkably constant across the series, with the average Y-O distance larger than that of Os-O. The contraction in the average A-site cation size is accommodated by the structure by the introduction of cooperative rotation of the corner-sharing octahedra. Four phases were identified and the sequence of these, together with their Glazer [49] tilt pattern is: $Fm\bar{3}m\,(a^0a^0a^0) \rightarrow I4/m\,(a^0a^0a^-) \rightarrow I2/m\,(a^-a^-c^0) \rightarrow P2_1/n\,(a^-a^-c^+)$. The $Fm\bar{3}m \rightarrow I4/m$ and $I2/m \rightarrow P2_1/n$ transitions involve the introduction of a tilt about [001] and are allowed by group theory to be continuous, whereas the $I4/m \rightarrow I2/m$ transformation requires a reorientation of the out-of-phase tilt from [001] to [110] and is required to be first order. The variation of

the volume in the solid solution, plotted in the inset of Figure 9, shows evidence for a small anomaly near $x = 0.8\text{-}1.0$ that may be associated with the first order $I4/m \rightarrow I2/m$ transition.
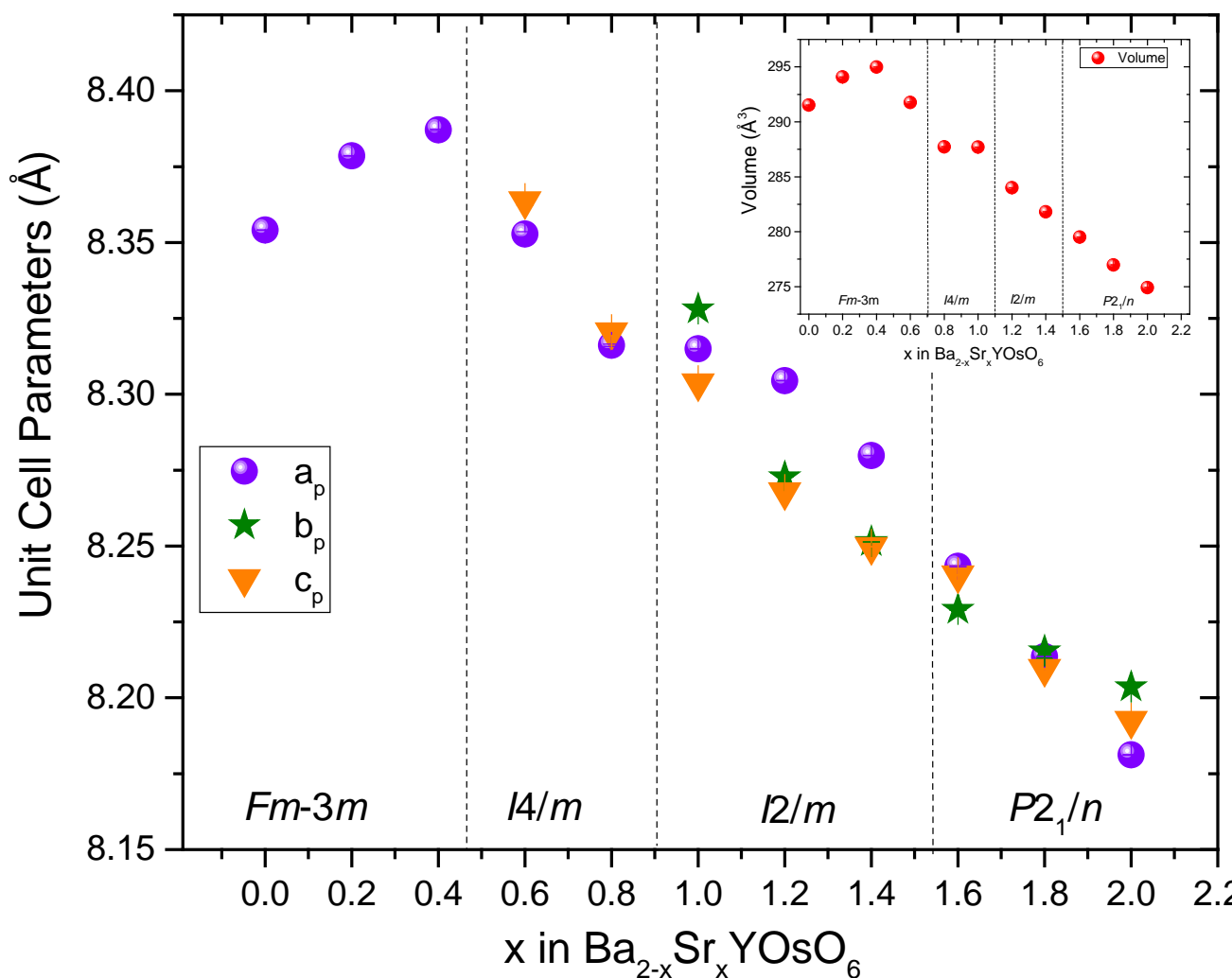
Figure 9. Composition dependence of the, appropriately scaled, unit-cell parameters and volume (inset) for the series $Ba_{2-x}Sr_xYOsO_6$ estimated by Rietveld refinements against combined S-XRD and NPD data sets. Where not apparent the esds in the values are smaller than the symbols.

The inclusion of the NPD data in the structural refinements provided relatively precise and accurate atomic coordinates for the anions, and hence for the individual bond distances and angles. As noted above the average Y-O and Os-O distances are remarkably constant

across the series. Internal changes in the structures are expected to directly impact the magnetic properties. The effect of the octahedral tilting on the Neel temperature is observed in Figure 10. A feature of this figure is that T_N reasonably constant for samples with monoclinic symmetry ($x < 1.4$) and then increases above this. This suggests there is a critical angle at which the favourable AFM superexchange interactions are maximised. In particular a decrease of the Y-O-Os bond angle leads to less effective overlap between $5d$-Os and $2p$-O orbitals and thus weakens the superexchange interactions. This results in a lowering of the magnetic ordering temperature.
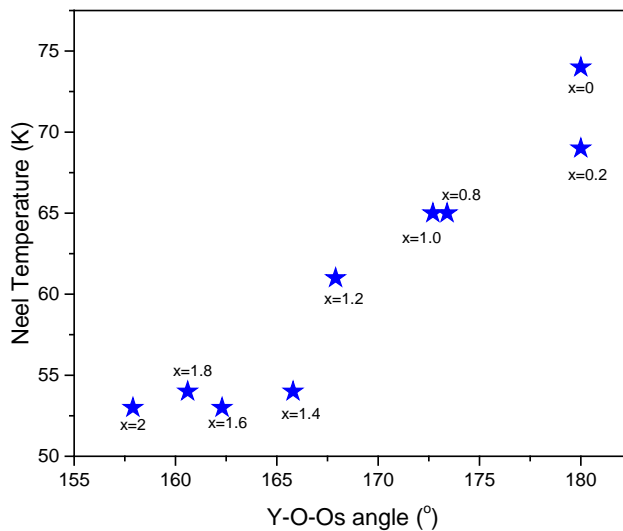
Figure 10. Variation of the Neel temperature versus the bond angle Y-O-Os for members of the series $Ba_{2-x}Sr_xYOsO_6$.

There are two possible superexchange pathways, via nearest neighbor (NN) Os-O-Os (π-superexchange) and next nearest neighbor interactions (NNN) Os-O-Y-O-Os (σ-superexchange). Since Os^{5+}, the only magnetic cations involved in the magnetic interactions, has a half-filled t_{2g} orbital set the NN interactions are expected to be AFM, as described by the Goodenough-Kanamori rules [50]. On the other hand, the coupling of two Os cations over the NNN Os−O−Y−O−Os linkage is dependent on the connection through the non-magnetic cation Y^{3+} (d^0). DFT calculations indicate that the NNN Os-O-Y-O-Os interactions are

weaker than the NN Os-O-Os interactions that are mediated by a π interaction.[51] The resulting competition between the magnetic interactions gives rise to the well-known AFM1 magnetic structure, [52, 53] where eight of the NN spins are AF aligned, four are FM, and all NNN spins are also FM. This is a very common spin arrangement previously described in numerous double perovskites including Sr_2YRuO_6 and it is consistent with the refined magnetic structure obtained at 3 K (Figure 5 and 6).

The values of the ordered magnetic moments estimated from the neutron diffraction, 1.5(2) and 1.64(5) μ_B for x = 1.0 and 1.2 respectively, are noticeably lower than those expected for S=3/2 Os^{+5} (μ = 3 μ_B) which in turn is lower than the theoretical spin only magnetic moment of 3.87 μ_B for the Os^{5+} (t_{2g}^3, S=3/2) ion. Considering the effects of SOC alone a moment of 1.9–2.3 μ_B for Os^{5+} appears reasonable [8]. That the observed moment is reduced from this suggests other effects such as covalency between the d and O p orbitals, which removes some fraction of the ordered moment from the transition metal ion site and transfers it to the ligand site or fluctuations induced by either geometrical or quantum effects may also be important. Since one of the cations placed over the B-site is non-magnetic (Y^{3+}), the Os^{5+} sublattice forms a fcc geometrically frustrated network and the dominating NN interactions between these cations are therefore frustrated. The frustration index is estimated to be $|\theta_{cw}|/T_N \sim$ 4-8 indicates a degree of frustration, but this alone is probably insufficient to explain the reduced magnetic moment. The large covalence of the Os-O chemical bonds caused by the spatially extended $5d$ orbitals results in a high delocalization of the magnetic moments and it might contribute to lower the experimental magnetic moment. X-ray absorption spectroscopy shows that the branching ratio $I(L_3)/I(L_2)$, is constant across the series. This implies that the magnitude of the SOC is also relatively constant. That SOC plays a significant role in the reduction of the magnetic moments has been identified from inelastic neutron experiment on similar systems. Kanungo et $al.$ [54] have investigated the magnetic properties of related Os containing-perovskites (Sr_2BOsO_6, B = Y, Sc and In) using first-principles density functional theory and they concluded that SOC is essential to describe the magnetic behavior of the mentioned compounds. Initially, they found the AFM2 structure to be the preferred magnetic ground state, however, including SOC in their calculations results in AFM1 state being energetically lower than AFM2 by a value ~1.2 meV/f.u. Furthermore, Taylor et $al.$ [51] have reported the presence of a large spin gap in the Sr_2ScOsO_6. It evidences the existence of SOC-induced anisotropy which is indispensable to stabilize the AFM1 ground state of a fcc frustrated system with strong NN magnetic interactions and negligible

NNN interactions. Since there are many factors involved in the stabilization of the magnetic ground state of the current systems it would be interesting to further analyze the system as a function of changing symmetry theoretically.

CONCLUSIONS

Accurate and precise structures have been determined for 11 members in the series $Ba_{2-x}Sr_xYOsO_6$ using a combination of synchrotron X-ray and neutron powder diffraction methods. The results obtained from the Rietveld refinement using combined S-XRD and NPD data sets show the structure to evolve from cubic to monoclinic as the Sr content is increased due to the introduction of cooperative tilting of the octahedra. Bulk magnetic susceptibility measurements reveal a, non-linear, increase in the Neel Temperature demonstrating the sensitivity of the magnetic ground state to changes in the precise nature of the structure, and in particular the Os-O-Y-O-Os geometry. The bulk magnetic moments are significantly reduced from the corresponding spin only value. The Os L_3:L_2 branching ratio $= I(L_3)/I(L_2) \sim 2.2$ was only slightly above the statistical value of 2 and constant across the series as determined by X-ray absorption spectra demonstrating both that the SOC does not change across the series and is relatively unimportant. This indicates that in the current series the observed reduction in reduced magnetic moment from the spin-only value can be attributed to covalence effects rather than SOC. This observation is inconsistent with the recent inelastic neutron study by Kermarrec et al.[8] that identified an unexpected spin gap that they proposed was a consequence of SOC. Additional studies are required to reconcile these differences.

Table 1. Unit-cell, atomic positions, thermal parameters, and reliability factors for $Ba_{2-x}Sr_xYOsO_6$ obtained from the combined refinements S-XRD and NPD data at room temperature. The magnetic parameters for selected members of the solid solution were obtained from the susceptibility measurements.

S.G:	$Fm\bar{3}m$			$I4/m$		$I2/m$			$P2_1/n$		
x	**0**	**0.2**	**0.4**	**0.6**	**0.8**	**1.0**	**1.2**	**1.4**	**1.6**	**1.8**	**2.0**
a (Å)	8.35409(1)	8.37852(8)	8.3871(2)	5.9063(8)	5.8804(4)	5.87957(9)	5.87216(4)	5.85472(3)	5.8289(2)	5.80788(3)	5.78499(8)
b (Å)						5.8888(1)	5.84971(4)	5.83460(3)	5.8188(2)	5.80914(3)	5.80075(7)
c (Å)				8.3637(14)	8.3205(12)	8.3037(1)	8.26782(5)	8.24978(5)	8.2404(2)	8.20959(4)	8.1925(1)
β (°)						90.1889(9)	90.1334(6)	90.1538(4)	90.146(2)	90.1761(3)	90.1811(8)
V (Å³)	583.038(2)	588.169(1)	589.97(1)	291.76(7)	287.72(5)	287.505(7)	284.003(3)	281.811(3)	279.50(1)	276.980(2)	274.917(6)
A x						0.4979(6)	0.4996(4)	0.4978(4)	0.0030(11)	0.0047(3)	0.0017(5)
y									0.4868(4)	0.4789(2)	0.47311(2)
z						0.2502(8)	0.2524(2)	0.2513(2)	0.248 (1)	0.2480(2)	0.2535(5)
B (Å²)	0.508(6)	0.466(16)	0.77(3)	1.09(3)	0.656(9)	0.58 (1)	0.659(8)	0.921(8)	0.845(16)	0.710(13)	0.841(14)
Y B (Å²)	0.144(9)	0.04(3)	0.68(6)	0.56(9)	0.196(16)	0.37(2)	0.143(6)	0.253(11)	0.189(16)	0.094(6)	0.186(11)
Os B (Å²)	0.146(5)	0.13(1)	0.54(2)	0.60(7)	0.248(8)	0.23(1)	0.133(13)	0.219(6)	0.075(9)	0.094(6)	0.117(6)
O1 x						-0.022(2)	-0.040(1)	-0.0549(11)	0.0526(17)	0.0613(12)	0.0702(15)
y									0.007(2)	0.0103(14)	0.0187(13)
z	0.2341(3)	0.2327(4)	0.2319(5)	0.234(3)	0.230(4)	0.2365(14)	0.2335(9)	0.2376(10)	0.2373(13)	0.2455(9)	0.2312(11)
B (Å²)	0.73(2)	0.82(5)	1.32(7)	1.7(5)	2.2(4)	0.8(2)	1.1(2)	1.50(16)	1.26(16)	0.42(11)	0.79(16)
O2 x				0.222(2)	0.217(2)	0.248(2)	0.2274(7)	0.2338(7)	0.2067(17)	0.204(2)	0.2061(17)
y				0.246(2)	0.260(2)	0.218(2)	0.2416(9)	0.2342(9)	0.2588(19)	0.2527(19)	0.2656(16)
z						0.005 (1)	0.0241(6)	0.0268(5)	-0.0289(12)	-0.0283(13)	-0.0398(15)
B (Å²)				1.3(2)	0.8 (1)	1.4 (1)	1.22(11)	1.33(9)	0.55(16)	2.1(2)	0.87(16)
O3 x									0.2586(16)	0.2767(17)	0.2776(18)
y									0.7897(12)	0.8143(9)	0.7988(12)
x									-0.0321(12)	-0.0076(9)	-0.0231(12)
B (Å²)									0.55(16)	0.28(14)	0.71(16)
Reliability Factors											
χ2	5.42	8.83	5.6	3.08	5.07	3.82	3.35	3.23	10.2	3.72	3.75
Magnetic Parameters											
T_N (K)	69	74			65	65	61	54	53	54	53
θ (K)	-717	-497			-460	-528	-354	-355	-365	-497	-313

Table 2. Main bond distances (Å) and selected angles (°) for $Ba_{2-x}Sr_xYOsO_6$, obtained from Rietveld refinements against combined S-XRD and NPD data sets at room temperature

| S.G:	$Fm\bar{3}m$			$I4/m$			$I2/m$		$P2_1/n$		
x	0	0.2	0.4	0.6	0.8	1.0	1.2	1.4	1.6	1.8	2.0
Os-O1 (Å)	1.956(2)	1.950(3)	1.945(4)	1.95(2)	1.91(3)	1.97(1)	1.946(7)	1.987(8)	1.979(11)	2.046(7)	1.939(9)
Os-O2 (Å)				1.952(10)	1.991(12)	1.948(1)	1.954(5)	1.946(5)	1.944(11)	1.901(11)	1.976(10)
Os-O3 (Å)									1.960(9)	1.937(9)	1.995(9)
Os-O$_{av}$ (Å)	**1.956(2)**	**1.950(3)**	**1.945(4)**	**1.95(1)**	**1.96(1)**	**1.95(1)**	**1.951(6)**	**1.960(6)**	**1.961(10)**	**1.961(9)**	**1.970(9)**
Y-O1 (Å)	2.221(2)	2.240(3)	2.249(4)	2.21(2)	2.25(3)	2.20(12)	2.216(7)	2.188(8)	2.188(11)	2.121(7)	2.243(9)
Y-O2 (Å)				2.215(10)	2.182(12)	2.221(12)	2.211(5)	2.210(5)	2.224(10)	2.252(11)	2.201(10)
Y-O3 (Å)									2.211(8)	2.240(7)	2.167(8)
Y-O$_{av}$ (Å)	**2.221(2)**	**2.240(3)**	**2.249(4)**	**2.21(7)**	**2.20(3)**	**2.214(12)**	**2.213(6)**	**2.202(7)**	**2.207(10)**	**2.204(8)**	**2.203(9)**
Y-O1-Os (°)	180	180	180	180	180	172.8(5)	166.8(3)	162.2(3)	162.9(4)	160.0(3)	156.7(4)
Y-O2-Os (°)				174.3(5)	170.1(5)	172.7(5)	168.5(2)	167.7(2)	162.2(4)	162.9(4)	157.5(4)
Y-O3-Os (°)									161.7(3)	159.0(3)	159.7(3)
Y-O-Os$_{avg}$ (°)	**180**	**180**	**180**	**176.2(9)**	**173.4(5)**	**172.7(5)**	**167.9(2)**	**165.8(2)**	**162.3(3)**	**160.6(3)**	**157.9(4)**

References

(1)   Ray, S.; Kumar, A.; Majumdar, S.; Sampathkumaran, E. V.; Sarma, D. D. Transport and magnetic properties of $Sr_2FeMo_xW_{1-x}O_6$. *J. Phys.: Condens. Matter* **2001,** 13, 607-616.

(2)   Das, H.; De Raychaudhury, M.; Saha-Dasgupta, T. Moderate to large magneto-optical signals in high T_c double perovskites. *Appl. Phys. Lett.,* **2008,** 92, 201912.

(3)   Krockenberger, Y.; Mogare, K.; Reehuis, M.; Tovar, M.; Jansen, M.; Vaitheeswaran, G.; Kanchana, V.; Bultmark, F.; Delin, A.; Wilhelm, F.; Rogalev, A.; Winkler, A.; Alff, L. Sr_2CrOsO_6: End point of a spin-polarized metal-insulator transition by 5d band filling. *Phys. Rev. B,* **2007,** 75, 020404.

(4)   Philipp, J. B.; Majewski, P.; Alff, L.; Erb, A.; Gross, R.; Graf, T.; Brandt, M. S.; Simon, J.; Walther, T.; Mader, W.; Topwal, D.; Sarma, D. D. Structural and doping effects in the half-metallic double perovskite A_2CrWO_6 (A = Sr, Ba, and Ca). *Phys. Rev. B,* **2003,** 68, 144431.

(5)   Kato, H.; Okuda, T.; Okimoto, Y.; Tomioka, Y.; Takenoya, Y.; Ohkubo, A.; Kawasaki, M.; Tokura, Y. Metallic ordered double-perovskite Sr_2CrReO_6 with maximal Curie temperature of 635 K. *Appl. Phys. Lett.,* **2002,** 81, 328-330.

(6)   Anderson, M. T.; Greenwood, K. B.; Taylor, G. A.; Poeppelmeier, K. R. B-cation arrangements in double perovskites. *Progress Solid State Chem.,* **1993,** 22, 197-233.

(7)   Vasala, S.; Karppinen, M. $A_2B'B''O_6$ perovskites: A review. *Progress Solid State Chem.,* **2015,** 43, 1-36.

(8)   Kermarrec, E.; Marjerrison, C. A.; Thompson, C. M.; Maharaj, D. D.; Levin, K.; Kroeker, S.; Granroth, G. E.; Flacau, R.; Yamani, Z.; Greedan, J. E.; Gaulin, B. D. Frustrated fcc antiferromagnet Ba_2YOsO_6: Structural characterization, magnetic properties, and neutron scattering. *Phys. Rev. B,* **2015,** 91.

(9)   Nilsen, G. J.; Thompson, C. M.; Ehlers, G.; Marjerrison, C. A.; Greedan, J. E. Diffuse magnetic neutron scattering in the highly frustrated double perovskite Ba_2YRuO_6. *Phys. Rev. B,* **2015,** 91, 054415.

(10)   Morrow, R.; Mishra, R.; Restrepo, O. D.; Ball, M. R.; Windl, W.; Wurmehl, S.; Stockert, U.; Buechner, B.; Woodward, P. M. Independent Ordering of Two Interpenetrating Magnetic Sublattices in the Double Perovskite Sr_2CoOsO_6. *J. Am. Chem. Soc.,* **2013,** 135, 18824-18830.

(11)   Yan, B.; Paul, A. K.; Kanungo, S.; Reehuis, M.; Hoser, A.; Toebbens, D. M.; Schnelle, W.; Williams, R. C.; Lancaster, T.; Xiao, F.; Moeller, J. S.; Blundell, S. J.; Hayes, W.; Felser, C.; Jansen, M. Lattice Site Specific Spin Dynamics in Double Perovskite Sr_2CoOsO_6. *Phys. Rev. Lett.,* **2014,** 112, 147202.

(12)   Kanungo, S.; Yan, B.; Jansen, M.; Felser, C. Ab initio study of low-temperature magnetic properties of double perovskite Sr_2FeOsO_6. *Phys. Rev. B,* **2014,** 89, 214414.

(13)   Paul, A. K.; Reehuis, M.; Ksenofontov, V.; Yan, B.; Hoser, A.; Toebbens, D. M.; Abdala, P. M.; Adler, P.; Jansen, M.; Felser, C. Lattice Instability and Competing Spin Structures in the Double Perovskite Insulator Sr_2FeOsO_6. *Phys. Rev. Lett.,* **2013,** 111, 167205.

(14)   Paul, A. K.; Sarapulova, A.; Adler, P.; Reehuis, M.; Kanungo, S.; Mikhailova, D.; Schnelle, W.; Hu, Z.; Kuo, C.; Siruguri, V.; Rayaprol, S.; Soo, Y.; Yan, B.; Felser, C.; Tjeng, L. H.; Jansen, M. Magnetically Frustrated Double Perovskites: Synthesis, Structural Properties, and Magnetic Order of Sr_2BOsO_6 (B = Y, In, Sc). *Z. Anorg. Allg. Chem.,* **2015,** 641, 197-205.

(15)   Taylor, A. E.; Morrow, R.; Singh, D. J.; Calder, S.; Lumsden, M. D.; Woodward, P. M.; Christianson, A. D. Magnetic order and electronic structure of the $5d^3$ double perovskite Sr_2ScOsO_6. *Phys. Rev. B,* **2015,** 91, 100406.

(16)   Morrow, R.; Soliz, J. R.; Hauser, A. J.; Gallagher, J. C.; Susner, M. A.; Sumption, M. D.; Aczel, A. A.; Yan, J. Q.; Yang, F. Y.; Woodward, P. M. The effect of chemical pressure on the structure and properties of A_2CrOsO_6 (A = Sr, Ca) ferrimagnetic double perovskite. *J. Solid State Chem. ,* **2016,** 238, 46-52.

(17)   Samanta, K.; Sanyal, P.; Saha-Dasgupta, T. Half-Metallic Behavior in Doped Sr_2CrOsO_6 Double Perovskite with High Transition Temperature. *Sci. Rep.,* **2015,** 5, 15010.

(18)   Saad, M. Electronic, magnetic, and optical characteristics of half-semiconductor double perovskite oxide Sr_2CrOsO_6 governed by 3d $(t_{2g})^3$-5d $(t_{2g})^3$ antiferromagnetic coupling. *J. Phys. Chem. Solids,* **2016,** 94, 1-11.

(19)   Russell, D. D.; Neer, A. J.; Melot, B. C.; Derakhshan, S. Long-Range Antiferromagnetic Ordering in B-Site Ordered Double Perovskite Ca_2ScOsO_6. *Inorg. Chem.,* **2016,** 55, 2240-2245.

(20)   Feng, H. L.; Schnelle, W.; Tjeng, L. H.; Jansen, M. Synthesis, crystal structures, and magnetic properties of double perovskites $SrLaNiOsO_6$ and $BaLaNiOsO_6$. *Solid State Commun.,* **2016,** 243, 49-54.

(21)   Thompson, C. M.; Marjerrison, C. A.; Sharma, A. Z.; Wiebe, C. R.; Maharaj, D. D.; Sala, G.; Flacau, R.; Hallas, A. M.; Cai, Y.; Gaulin, B. D.; Luke, G. M.; Greedan, J. E. Frustrated Magnetism In The Double Perovskite La_2LiOsO_6: A Comparison With La_2LiRuO_6. *Phys. Rev. B,* **2016,** 93, 014431.

(22)   Kim, B. J.; Jin, H.; Moon, S. J.; Kim, J. Y.; Park, B. G.; Leem, C. S.; Yu, J.; Noh, T. W.; Kim, C.; Oh, S. J.; Park, J. H.; Durairaj, V.; Cao, G.; Rotenberg, E. Novel J(eff)=1/2 Mott state induced by relativistic spin-orbit coupling in Sr_2IrO_4. *Phys. Rev. Lett.,* **2008,** 101, 076402.

(23)   Calder, S.; Vale, J. G.; Bogdanov, N. A.; Liu, X.; Donnerer, C.; Upton, M. H.; Casa, D.; Said, A. H.; Lumsden, M. D.; Zhao, Z.; Yan, J. Q.; Mandrus, D.; Nishimoto, S.; van den Brink, J.; Hill, J. P.; McMorrow, D. F.; Christianson, A. D. Spin-orbit-driven magnetic structure and excitation in the 5d pyrochlore $Cd_2Os_2O_7$. *Nat. Commun.,* **2016,** 7, 11651.

(24)   Wallwork, K. S.; Kennedy, B. J.; Wang, D. The High Resolution Powder Diffraction Beamline For The Australian Synchrotron. *AIP Conference Proceedings,* **2007,** 879, 879-882.

(25)   Studer, A. J.; Hagen, M. E.; Noakes, T. J. Wombat: The high-intensity powder diffractometer at the OPAL reactor. *Physica B,* **2006,** 385–386, 1013-1015.

(26)   Liss, K.-D.; Hunter, B.; Hagen, M.; Noakes, T.; Kennedy, S. Echidna - the new high-resolution powder diffractometer being built at OPAL. *Physica B,* **2006,** 385-86, 1010-1012.

(27)   Rietveld, H. M. A Profile Refinement Method For Nuclear And Magnetic Structures. *J. Appl. Crystallogr.,* **1969,** 2, 65.

(28)   Rodriguez-Carvajal, J. Recent Advances In Magnetic-Structure Determination By Neutron Powder Diffraction. *Physica B,* **1993,** 192, 55-69.

(29)   Glover, C.; McKinlay, J.; Clift, M.; Barg, B.; Boldeman, J.; Ridgway, M.; Foran, G.; Garrett, R.; Lay, P.; Broadbent, A. Status of the x-ray absorption spectroscopy (XAS) beamline at the Australian synchrotron. *AIP Conference Proceedings,* **2007,** 882, 884-886.

(30)   Ravel, B.; Newville, M. ATHENA, ARTEMIS, HEPHAESTUS: data analysis for X-ray absorption spectroscopy using IFEFFIT. *J. Synchrot. Radiat.,* **2005,** 12, 537-541.

(31)   Howard, C. J.; Kennedy, B. J.; Woodward, P. M. Ordered double perovskites - a group-theoretical analysis. *Acta Crystallogr. Sect. B-Struct. Sci.,* **2003,** 59, 463-471.

(32)   Zhou, Q.; Kennedy, B. J.; Elcombe, M. M. Composition And Temperature Dependent Phase Transitions In Co–W Double Perovskites, A Synchrotron X-Ray And Neutron Powder Diffraction Study. *J. Solid State Chem. ,* **2007,** 180, 541-548.

(33)   Ranjbar, B.; Pavan, A.; Kennedy, B. J.; Zhang, Z. M. Structural and magnetic properties of the ruthenium double perovskites $Ba_{2-x}Sr_xYRuO_6$. *Dalton Trans.,* **2015,** 44, 10689-10699.

(34)   Ranjbar, B.; Reynolds, E.; Kayser, P.; Kennedy, B. J.; Hester, J. R.; Kimpton, J. A. Structural and Magnetic Properties of the Iridium Double Perovskites $Ba_{2-x}Sr_xYIrO_6$. *Inorg. Chem.,* **2015,** 54, 10468-10476.

(35)   Zhou, Q. D.; Kennedy, B. J.; Elcombe, M. M. Composition And Temperature Dependent Phase Transitions In Co-W Double Perovskites, A Synchrotron X-Ray And Neutron Powder Diffraction Study. *J. Solid State Chem. ,* **2007,** 180, 541-548.

(36)   Zhou, Q. D.; Kennedy, B. J.; Howard, C. J.; Elcombe, M. M.; Studer, A. J. Structural phase transitions in $A_2Sr_xNiWO_6$ (A = Ca or Ba, 0 < x < 2) double perovskites. *Chem. Mater. ,* **2005,** 17, 5357-5365.

(37)   Zhou, Q. D.; Tan, T. Y.; Kennedy, B. J.; Hester, J. R. Crystal structures and phase transitions in Sr doped Ba_2InTaO_6 perovskites. *J. Solid State Chem. ,* **2013,** 206, 122-128.

(38)   Ramirez, A. P. Strongly Geometrically Frustrated Magnets. *Annu. Rev. Mater. Sci.,* **1994,** 24, 453-480.

(39)   Bertaut, E. F., *Magnetism* Academic Press: New York, 1963; Vol. 3.

(40)   Zhang, Z. M.; Middleburgh, S. C.; de los Reyes, M.; Lumpkin, G. R.; Kennedy, B. J.; Blanchard, P. E. R.; Reynolds, E.; Jang, L. Y. Gradual Structural Evolution from Pyrochlore to Defect-Fluorite in $Y_2Sn_{2-x}Zr_xO_7$: Average vs Local Structure. *J. Phys. Chem. C,* **2013,** 117, 26740-26749.

(41)   Zhang, Z. M.; Avdeev, M.; de los Reyes, M.; Lumpkin, G. R.; Kennedy, B. J.; Blanchard, P. E. R.; Liu, S.; Tadich, A.; Cowie, B. C. C. Probing Long- and Short-Range Disorder in $Y_2Ti_{2-x}Hf_xO_7$ by Diffraction and Spectroscopy Techniques. *J. Phys. Chem. C,* **2016,** 120, 26465-26479.

(42)   Krause, M. O.; Oliver, J. H. Natural widths of atomic K-levels and L-levels, K-alpha x-ray-lines and several KLL Auger lines. *J. Phys. Chem. Ref. Data,* **1979,** 8, 329-338.

(43)   Laguna-Marco, M. A.; Kayser, P.; Alonso, J. A.; Martinez-Lope, M. J.; van Veenendaal, M.; Choi, Y.; Haskel, D. Electronic structure, local magnetism, and spin-orbit effects of Ir(IV)-, Ir(V)-, and Ir(VI)-based compounds. *Phys. Rev. B,* **2015,** 91, 214433.

(44)   Thole, B. T.; Vanderlaan, G. Branching Ratio In X-Ray Absorption-Spectroscopy. *Phys. Rev. B,* **1988,** 38, 3158-3171.

(45)   Clancy, J. P.; Chen, N.; Kim, C. Y.; Chen, W. F.; Plumb, K. W.; Jeon, B. C.; Noh, T. W.; Kim, Y. J. Spin-Orbit Coupling In Iridium-Based 5d Compounds Probed By X-Ray Absorption Spectroscopy. *Phys. Rev. B,* **2012,** 86, 195131.

(46)   Cho, D. Y.; Park, J.; Yu, J.; Park, J. G. X-ray absorption spectroscopy studies of spin-orbit coupling in 5d transition metal oxides. *J. Phys.: Condens. Matter* **2012,** 24, 7.

(47)   Zhou, Q. D.; Kennedy, B. J.; Kimpton, J. A. The effect of disorder in Ba_2YTaO_6 on the tetragonal to cubic phase transition. *J. Solid State Chem.,* **2011,** 184, 729-734.

(48)   Carpenter, M. A.; McKnight, R. E. A.; Howard, C. J.; Zhou, Q. D.; Kennedy, B. J.; Knight, K. S. Characteristic length scale for strain fields around impurity cations in perovskites. *Phs. Rev. B,* **2009,** 80, 214101.

(49)   Glazer, A. M. Classification of tilted octahedra in perovskites. *Acta Crystallogr. Sect. B-Struct. Sci.,* **1972,** B 28, 3384.

(50)   Goodenough, J. B., *Magnetism and the Chemical Bond*. R. E. Krieger Pub. Co.: Malabar, FL, 1976.

(51)   Taylor, A. E.; Morrow, R.; Fishman, R. S.; Calder, S.; Kolesnikov, A. I.; Lumsden, M. D.; Woodward, P. M.; Christianson, A. D. Spin-orbit coupling controlled ground state in Sr_2ScOsO_6. *Phys. Rev. B,* **2016,** 93, 100406.

(52)   Aczel, A. A.; Bugaris, D. E.; Li, L.; Yan, J. Q.; de la Cruz, C.; zur Loye, H. C.; Nagler, S. E. Frustration by competing interactions in the highly distorted double perovskites $La_2NaB'O_6$ (B ' = Ru, Os). *Phys. Rev. B,* **2013,** 87.

(53)   Battle, P. D.; Macklin, W. J. The crystal and magnetic structures of Sr_2YRuO_6. *J. Solid State Chem. ,* **1984,** 52, 138-145.

(54)   Kanungo, S.; Yan, B. H.; Felser, C.; Jansen, M. Active role of nonmagnetic cations in magnetic interactions for double-perovskite Sr_2BOsO_6(B = Y, In, Sc). *Phys. Rev. B,* **2016,** 93, 161116.

-Table of Contents-
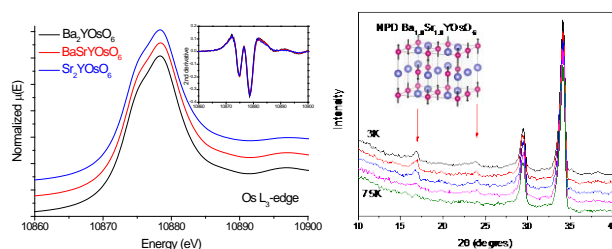
The impact of chemical doping on the structures and magnetic properties of the ordered double perovskites $Ba_{2-x}Sr_xYOsO_6$ was investigated using neutron and X-ray diffraction, X-ray spectroscopy and bulk magnetic susceptibilities. The structure to evolve from cubic to monoclinic as the Sr content is increased. The oxide all have a AFM1 type magnetic structure and analysis of the Os L_3:L_2 branching ratio, as determined by X-ray absorption spectra, shows that the spin-orbit coupling is constant across the series.